

## Two-State Membrane Potential Fluctuations Driven by Weak Pairwise Correlations

**Andrea Benucci**

*andrea@ski.org*

**Paul F.M.J. Verschure**

*pfnjv@ini.phys.ethz.ch*

**Peter König**

*pkoenig@uni-osnabrueck.de*

*Institute of Neuroinformatics University and ETH Zürich 8057 Zürich, Switzerland*

Physiological experiments demonstrate the existence of weak pairwise correlations of neuronal activity in mammalian cortex (Singer, 1993). The functional implications of this correlated activity are hotly debated (Roskies et al., 1999). Nevertheless, it is generally considered a widespread feature of cortical dynamics. In recent years, another line of research has attracted great interest: the observation of a bimodal distribution of the membrane potential defining up states and down states at the single cell level (Wilson & Kawaguchi, 1996; Steriade, Contreras, & Amzica, 1994; Contreras & Steriade, 1995; Steriade, 2001). Here we use a theoretical approach to demonstrate that the latter phenomenon is a natural consequence of the former. In particular, we show that weak pairwise correlations of the inputs to a compartmental model of a layer V pyramidal cell can induce bimodality in its membrane potential. We show how this relationship can account for the observed increase of the power in the  $\gamma$ -frequency band during up states, as well as the increase in the standard deviation and fraction of time spent in the depolarized state (Anderson, Lampl, Reichova, Carandini, & Ferster, 2000). In order to quantify the relationship between the correlation properties of a cortical network and the bistable dynamics of single neurons, we introduce a number of new indices. Subsequently, we demonstrate that a quantitative agreement with the experimental data can be achieved, introducing voltage-dependent mechanisms in our neuronal model such as  $\text{Ca}^{2+}$ - and  $\text{Ca}^{2+}$ -dependent  $\text{K}^+$  channels. In addition, we show that the up states and down states of the membrane potential are dependent on the dendritic morphology of cortical neurons. Furthermore, bringing together network and single cell dynamics under a unified view allows the direct transfer of results obtained in one context to the other and suggests a new experimental paradigm: the use of specific intracellular analysis as a powerful tool to reveal the properties of the correlation structure present in the network dynamics.

## 1 Introduction

---

In this study, we address the relationship of two experimentally observed phenomena. At the network level, correlated spiking activity between ensembles of neurons has been described in recent years. At the cellular level, the observation that the membrane potential dynamics of single neurons can show distinct up states and down states has received a lot of attention.

Regarding the first phenomenon, multielectrode recordings in cat visual cortex have demonstrated that pairs of neurons sharing similar orientation tuning properties tend to have synchronized spiking activity (Singer, 1993). This finding has been confirmed in different species (Bair, 1999) and different cortical areas (Salinas & Sejnowski, 2001). The synchronization pattern is dependent on the properties of the stimulus. For example, when coherently moving gratings or randomly moving dots are used as visual stimuli, they elicit cortical activity that displays pairwise correlations of different degree (Gray, Engel, König, & Singer, 1990, Usrey & Reid, 1999). Moreover, cross-correlation analysis shows that rather than having a precise synchronization, optimally driven neurons lead over suboptimally driven ones (König, Engel, & Singer, 1995a) (see Figure 1B). This suggests that under realistic conditions, cortical dynamics is highly structured in the temporal domain (Roskies et al., 1999).

The impact of a large number of randomly timed or synchronized inputs on the subthreshold dynamics of single neurons has been studied in simulations (Salinas & Sejnowski, 2000; Bernander, Koch, & Usher, 1994; Destexhe & Paré, 1999; Shadlen & Newsome, 1998; Softky & Koch, 1993). However, taking into account our current knowledge of the correlation structure of cortical activity, we have little insight into the cellular dynamics under realistic conditions (Singer, 1993; Lampl, Reichova, & Ferster, 1999; Douglas, Martin, & Whitteridge, 1991; Stern, Kincaid, & Wilson, 1997; Agmon-Snir & Segev, 1993; Mel, 1993; Destexhe & Paré, 2000; Singer & Gray, 1995).

Regarding the second phenomenon, a number of intracellular studies have shown that the membrane potential of neurons does not take on any value between rest and threshold with equal probability but rather that it assumes either a depolarized state, associated with spiking activity, or a resting state where the cell is silent (see Figures 2A and 2B, right panels). This behavior has been observed in different animals and brain structures (Anderson, Lampl, Reichova, Carandini, & Ferster, 2000; Stern, Jaeger, & Wilson, 1998; Steriade, Timofeev, & Grenier, 2001). This bistability of the membrane potential is referred to as up states and down states, and its biophysical properties have been characterized (Wilson & Kawaguchi, 1996; Lampl et al., 1999; Douglas et al., 1991; Stern et al., 1997; Lewis & O'Donnell, 2000; Wilson & Groves, 1981; Kasanetz, Riquelme, & Murer, 2002) (see Figures 2A and 2B, right panels). The origin of up states and down states has been related to presynaptic events (Wilson & Kawaguchi, 1996); however, the underlying mechanisms have not yet been identified.

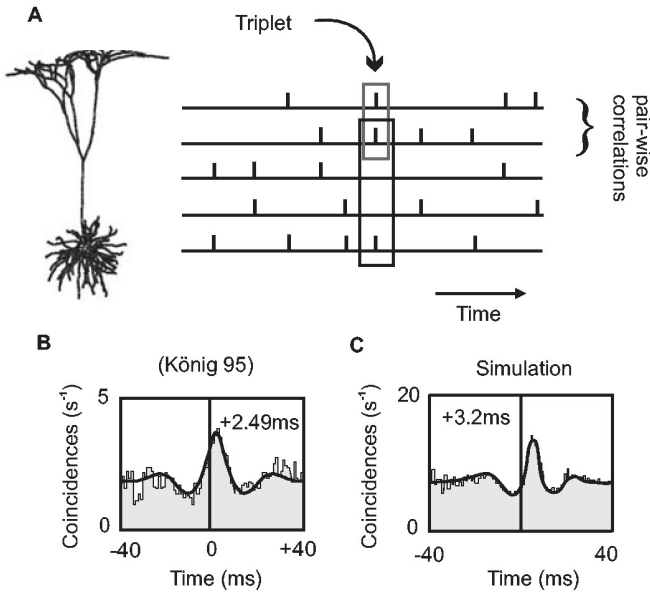
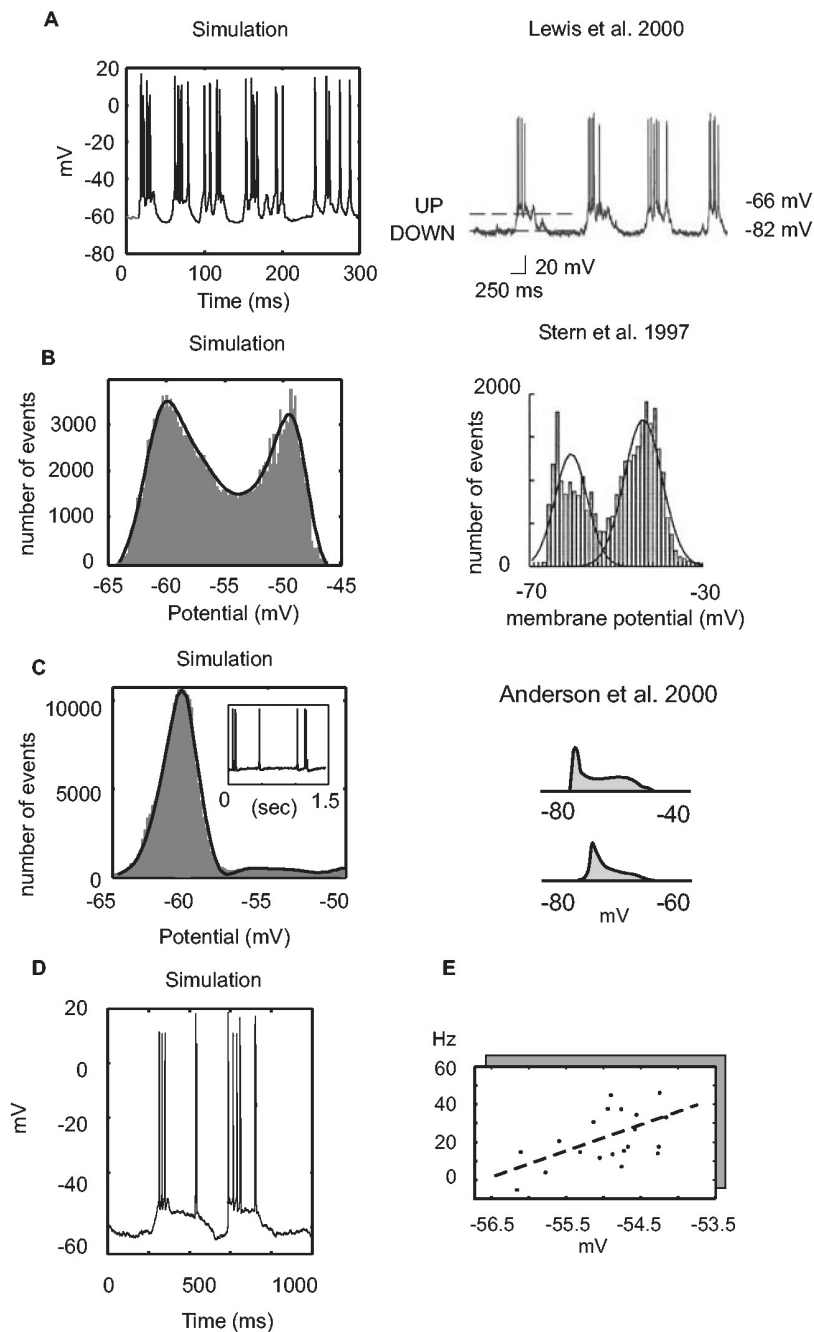


Figure 1: Model neuron and the temporal structure of its input. (A) Reconstructed layer 5 pyramidal cell (left) with a schematic of five input spike trains sharing weak pairwise correlations (right). For every pair of spike trains, there are moments in time when the probability of firing together is high and pairs of synchronized spikes occur. Due to the high level of input convergence, higher-order events emerge statistically and are shown as triplets in the example (Benucci et al., 2003). (B) Cross-correlation analysis of paired extracellular recordings from cat area 17 while using moving bars as visual stimuli (data taken from König et al., 1995a). The peak size is proportional to the strength of the correlation. The shift of the peak indicates a phase lag of the firing of one neuron relative to the other. In general, optimally driven cells tend to lead over suboptimally driven ones. Solid line: Gabor fit for parameters estimation. (C) Cross-correlogram of the synthetic data. Solid line: Gabor fit of the cross-correlogram.

Here, we take a theoretical approach to examine the dynamics of the membrane potential in single neurons given a physiologically constrained representation of the temporal properties of its afferent signals.

## 2 Materials and Methods

In the following, we describe a detailed model of a cortical neuron and a procedure to produce synthetic input spike trains with physiologically realistic first order (i.e., firing rates) and second-order statistical properties (i.e., pairwise correlations). Subsequently, our methods of analysis are introduced.



**2.1 The Cellular Model.** A morphologically detailed layer 5 pyramidal cell (Bernander, Koch, & Douglas, 1994; Bernander, Koch, & Usher, 1994; Destexhe & Paré, 2000) is simulated using the NEURON simulation environment (Hines & Carnevale, 2001) (see Figure 1A). (The original anatomical data are kindly made available by J. C. Anderson and K. A. C. Martin.) We deliberately keep the cell as simple as possible to avoid the introduction of strong a priori hypotheses. Nevertheless, the resulting simulated neuron is of considerable complexity. The parameters for the passive properties, HH-like channels in the soma and the synapses (4000 AMPA, 500 GABA<sub>a</sub>, 500 GABA<sub>b</sub>), are selected according to the available literature and previous computational studies (Bernander, Koch, & Douglas, 1994; Agmon-Snir & Segev, 1993; Bernander, Koch, & Usher, 1994; Mel, 1993; Destexhe & Paré, 2000). The parameter sets used are reported in Tables 1 through 3 (see the appendix). The files used to implement voltage-dependent mechanisms, as indicated in the tables, are freely available online from the NEURON web page (<http://www.neuron.yale.edu>). For the cell as a whole, we tune the parameters to obtain a consistent input-output firing-rate transfer function.

Figure 2: *Facing page.* Intracellular somatic recordings. (A) The membrane potential of the model neuron is shown during optimal stimulation (left panel). Spiking episodes (burst-like behavior) are associated with the depolarized states of the membrane potential (up states). Following spiking activity, there are periods in which the simulated cell is in a more hyperpolarized state and silent (down states). The pairwise correlation strength of the input spike trains has been set to 0.1 and the mean input firing rate to 85 Hz. The alternation between up states and down states has also been found in several experimental studies using intracellular recordings (right panel). (B) Histogram of the distribution of the membrane potential recorded under the conditions as shown in *a* after removal of the action potentials. The membrane potential does not take any value between the up states and down states with equal probability, but the histogram shows two peaks (left panel). Similarly, the biphasic behavior in the membrane potential has been experimentally observed (right panel). (C) If the cell in the simulation is stimulated solely by uncorrelated background activity (6 Hz), the bimodality disappears (left panel). The corresponding trace of the membrane potential is shown in the inset. Similar “shapes” in the histograms of the membrane potential under similar stimulation conditions have also been observed experimentally (right panel). Note that when not using visual stimulation, Anderson et al. (2000) found bimodal as well as nonbimodal distributions of the membrane potential. A nonbimodal example is shown here (see also section 4). (D) The duration of the up states has been increased 10 times with respect to Figure 2A due to the introduction of Ca<sup>2+</sup> and Ca<sup>2+</sup>-dependent K<sup>+</sup> channels in the modeled L5 pyramidal cell. (E) Relationship between the firing rate in the up states and the mean membrane potential with Ca<sup>2+</sup> and Ca<sup>2+</sup>-dependent K<sup>+</sup> currents. The input pairwise correlation strength is 0.1, and the mean input firing rate is 30 Hz.

Table 1: Simulation Parameters for the Active Mechanisms.

Ion	Current	Place	$E_{\text{rev}}$ (mV)	$\bar{G}$ (mS/cm <sup>2</sup> )	$p$	$q$	$\tau_{\text{act}}$ (ms)	$u_{1/2}$ (mV) (active/inactive)	$k$ (active/inactive)	File
Na <sup>+</sup>	I <sub>Na</sub>	Soma	50	500	2	1	0.05	-47/-42	3/-3	iaspec.mod
		Dendrites	50	10	2	1	0.05	-32/-37	3/-3	iap.mod
Ca <sup>2+</sup>	I <sub>L</sub>	Apical	115	5.1	2	0	2.12	-35	4	ical.mod
		Soma	-77	50	2	0	1.5	-47	3	iapspec.mod
K <sup>+</sup>	I <sub>C</sub>	Apical	-77	30	2	0	200	2.17		ic.mod
		Soma	-66	10	1	1	2	-24.5/-72.3	16.9/-5.9	ianew.mod
	I <sub>M</sub>	Dendrites	-66	10	1	1	2	-22.9/-83.1	16.2/-6.5	iA.mod
		Dendrites	-77	30	1	0	2.21-			km.mod
	I <sub>h</sub>	Apical	-50	L IV: 2.5	2	0	2.24	-68.9	-6.5	IH.mod
				L III: 7			2.26			
				L II: 22						
				L I: 32						

Table 2: Synaptic Parameters.

Type	$\bar{g}$ (nS)	$e_r$ (mV)	$\tau_1$ (ms)	$\tau_2$ (ms)	$\tau_{peak}$ (ms)
GABA <sub>a</sub>	1	-70	4.5	7	5.6
GABA <sub>b</sub>	0.1	-95	35	40	37.4
AMPA	20	0	0.3	0.4	0.35
NMDA	26.9	0	4	120	14

Table 3: Passive Properties.

$E_{rest}$	-65 mV
$C_m$	1 $\mu$ F
$G_m$	0.07 mS/cm <sup>2</sup>
$R_i$	90 $\Omega$ cm
$T$	36°C

**2.2 Input Stage, First-Order Statistics.** The input stage reproduces measured anatomical and physiological conditions (Douglas & Martin, 1990). Layer 5 neurons in cat's visual cortex do not receive significant input from the lateral geniculate nucleus; the overwhelming majority of inputs are cortico-cortical afferents (Gabbott, Martin, & Whitteridge, 1987). The distributions of orientation preferences of the afferent excitatory signals to our model neuron are graded and match the experimentally observed specificity of intra-areal corticocortical connections (Kisvarday, Toth, Rausch, & Eysel, 1997; Salin & Bullier, 1995): 57% of the inputs originate from neurons with similar ( $\pm 30$  degrees) orientation preference, and 30% and 13% of afferents originate from neurons with a preferred orientation differing by between 30 and 60 degrees and 60 and 90 degrees, respectively, from the neuron under consideration. This connectivity automatically provides the cell with a feedforward mechanism for its orientation tuning. Whether this mechanism correctly describes the origin of orientation-selective responses in primary visual cortex is still unresolved (Sompolinsky & Shapley, 1997) and not within the scope of this study. To take into account these physiological conditions, we separate the total of 5000 afferents of the simulated neuron according to the localization of the respective synapse in layer 1 to layer 5 into five groups. This gives the flexibility to make selective changes in the correlation properties of inputs targeting different cortical layers. Each of the five groups was subdivided into 36 subpopulations of afferents with similar orientation preference, resulting in a discretization of  $\pm 5$  degrees. This mimics the situation of input spike trains from cells having different tuning properties than the target neuron. The size of the subpopulations ranged linearly from 25 to 100 cells, for orthogonally tuned inputs to identically tuned inputs, respectively. The firing rates of the inputs are determined with a "typical" visual stimulus in mind (i.e., an oriented grat-

ing). The maximum input firing rate of the optimally stimulated neurons is set to 85 Hz. Nonoptimally stimulated cells are assumed to have an orientation tuning of  $\pm 30$  degrees half width at half height, and the firing rate is reduced accordingly. In addition, background activity is simulated with uniform, uncorrelated 6 Hz activity. Inhibitory inputs are implemented with a broader orientation tuning than excitatory inputs.

**2.3 Input Stage, Second-Order Statistics.** The rationale behind the synthetic spike train generation algorithm is that for each pair of spike trains, there are intervals in time when the probability of correlated spiking activity is increased. The method used closely resembles other published algorithms to produce correlated spike trains (Stroeve & Gielen, 2001; Feng & Brown, 2000), and the source code is available from the authors upon request. The statistical properties of the synthetic spike trains conform to known physiological constraints, such as average strength and precision of correlation, and for this reason, we will refer to them as physiologically realistic inputs. We do not introduce a dependence of the strength of correlation on the orientation tuning of the neurons. This conforms to the hypothesis that the synchronization patterns induced in the network reflect global stimulus properties and are not a fixed property of the network (Singer & Gray, 1995). In particular, when only a single stimulus is presented, the strength of synchronization of neuronal activity in the primary visual cortex over short distances is found not to depend on the orientation tuning of the neuron (Engel, König, Gray, & Singer, 1990).

The details of the algorithm are as follow: within the overall time window of analysis,  $T$  (typically 10 seconds), time epochs are selected, during which the probability of spiking is increased for all 5000 cells in the population afferent to the simulated neuron. Nevertheless, neurons spike only in correspondence to a subset of these epochs (randomly chosen), and for any two given cells, there is always a nonzero overlap between such subsets. The total number of possible overlaps depends, in a combinatorial way, on the size of the subsets, which is a controlled parameter of the simulation. It is the number and amount of these overlaps that determines the pairwise correlation strength and the different degrees of temporal alignments of the spikes. The epochs are time intervals centered on specific points in time, whose duration and distribution are controlled parameters of the algorithm.

We used a Poisson process to distribute these points in time, and their frequency was fixed at 75 Hz. The duration of the time epochs was 10 ms. The algorithm is very flexible; choosing a distribution other than a Poisson one (exponential or gamma of any order) would allow the creation of correlations with or without overall oscillatory activity (Gray & Viana di Prisco, 1997; Engel et al., 1990). The duration of the time epochs determines the precision of the correlations, and it can be changed to affect the overlaps between the epochs within the same spike train. The frequency of the time epochs is itself a free parameter. Spikes are assigned within the

epochs according to a distribution whose skewness and integral is parametrically controlled. The skewness controls the shape of the peaks in the cross-correlograms, with the possibility of creating very "sharp" or "broad" correlation peaks, without changing the correlation strength itself. In all the simulations, we used a gaussian distribution. The integral of the distribution controls the correlation strength. Thus, the absolute fraction of spikes assigned to the epochs changed depending on the desired pairwise correlation strength. The rest of the unassigned spikes are randomly distributed according to a Poisson process with constraints related to refractoriness (2 ms in the simulation). This ensures that the coefficient of variation (CV) of each spike train ranges around one (Dean, 1981). A key point of the simulation is that by varying the frequency and the duration of the time epochs, it is possible to create pairwise correlations in the population with different degrees of high-order correlation events (see the following section for more details). The temporal dynamics of the input stage thus reproduce in a controlled fashion the correlation strengths and time lags that have been observed experimentally.

In the following, the temporal precision of the correlations will be held constant, with the width of the peaks in the cross-correlograms always on the order of 10 ms. Furthermore, the time lags of the correlations are determined by a parameter that is kept fixed in all simulations (König, Engel, & Singer, 1995b). We vary only the correlation strength, that is, the height of the peaks in the cross-correlogram. We will refer to these dynamical features as to the correlation structure of the inputs (König, Engel, & Singer, 1995a; Roskies et al., 1999) (see Figures 1B and 1C). In our model, the inhibitory inputs follow the same correlation structure as the excitatory inputs. All simulations are analyzed in epochs of 10 s duration. For the quantitative evaluation of our data, we use a five-parameters Gabor fit of the cross-correlograms (König, 1994). We calculate the pairwise correlation strength as the area of the peak of the Gabor function divided by the area of the rectangular portion of the graph under the peak, delimited by the offset.

**2.4 Higher-Order Correlations.** Neuronal interactions in the cortex are measured solely in terms of correlations of the activity of pairs of neurons. Hence, the algorithm used here synthesizes spike trains with a specified pairwise correlation that satisfies those observed in the neuronal interactions in the cortex (see Figures 1B and 1C). Nevertheless, due to the high level of convergence observed in the cortex, higher-order statistical events must and do appear. This holds even for the low values of the experimentally observed pairwise correlations (Benucci, Vershure, & König, 2003; Destexhe & Paré, 2000; Bothé, Spekreijse, & Roelfsema, 2000; Grün, Diesmann, & Aertsen, 2001). Accordingly, the above-described algorithm not only generates weak pairwise correlations between the input spike trains, but also creates high-order correlations in the presynaptic population of neurons. Higher-

order events indicate episodes of the presynaptic dynamics characterized by spiking activity from a large fraction of afferent neurons, occurring altogether in a small time window on the order of a few milliseconds. How these nearly synchronized events naturally emerge from the pairwise correlations constraint, has been formally investigated (Benucci et al. 2003; Bothé et al., 2000). It can be intuitively understood considering that the number of pairwise coincidences rises quadratically with the number of afferents and that the number of spikes available to generate such coincidences rises only linearly with the number of afferents. It follows that spikes have to be “used” multiple times to generate coincidences; that is, higher-order correlations must appear. With an increasing number of inputs, the effect is amplified. This is important when considering realistic values for the number of afferent inputs to a given cortical cell, typically of the order of  $10^4$ . At this level of convergence, the statistical effect explained above becomes dominant, and higher-order events are a prominent feature of the dynamics (Mazurek & Shadlen, 2002).

**2.5 Analysis of Intracellular Dynamics.** The intracellular dynamics is evaluated using different measures in the time and frequency domain. The up states and down states of the subthreshold membrane potential are determined as in Anderson et al. (2000) using two thresholds. A sliding window of 50 ms is used to find segments in which the membrane potential is above the up threshold for more than 60% of the time. We use a similar procedure for identifying the down states (i.e., the membrane potential is below a down threshold). For the cumulative probability distribution of the membrane potential, any section where the membrane potential exceeds the up threshold is included in the analysis. To eliminate the spikes and check for the inverse relationship between the spike threshold and the slope of the rising phase of the action potential, we use the same procedure as in Azouz and Gray (2000). Furthermore, we compute a number of indices characterizing the relation of subthreshold dynamics with observable measures. These indices are defined in section 3.

**2.6 Control Simulations.** To verify the scope and robustness of the results found, we ran several simulations varying the values of the parameters. The rationale is that if a small change in the value of a given parameter causes a dramatic change in the results, then the mechanisms the parameter refers to should be considered critical for the emergence of the phenomenon studied. But if the changes are minor and smoothly affect the results, the associated mechanism is considered to be relevant for the modulation and quantitative features of the phenomenon, but not for the emergence of the effect per se.

We changed the width of the tuning curves of the inhibitions and excitations by a factor of  $\pm 10\%$  without noticing significant changes in the degree of bimodality. We also checked for the robustness of the results in

respect to changes in the time constants and conductance peak amplitudes of AMPA and GABA synapses. In the extreme cases of long time constants (NMDA synapses) and large (twice the mean) conductance amplitudes of AMPA synapses (see the tables for mean values), the cell was driven to an epileptic-like state. In case of GABA, the cell would be totally silenced. In between these extremes, the cell was showing smooth changes in the degree of bistable dynamics. We used exactly the same principles when performing controls with voltage-dependent mechanisms, such as calcium and sodium voltage-dependent currents, muscarinic channels, or anomalous rectifying currents (see the tables for complete listings of mechanisms used). We varied the values of the parameters around their means (as reported in the tables) and noticed only smooth modulatory effects. These controls confirm the generality of the phenomena as reported below.

Finally, for controls regarding the neuronal morphology, we used two strategies: we took a different cell model, and we reduced the whole cell, or part of the dendritic tree, to single equivalent compartments while keeping the electrotonic properties unaffected (Destexhe, 2001). The second cell model (a spiny stellate neuron) was kindly made available by Y. Banitt and I. Segev. It includes active mechanisms such as  $\text{Ca}^{2+}$  dynamics, fast repolarizing  $\text{K}^{+}$  currents,  $\text{Ca}^{2+}$ -dependent  $\text{K}^{+}$  currents, spike frequency adaptation, and  $\text{Na}^{+}$  channels, (parameters as in Banitt & Segev, personal communication, 2003). The input spike trains are generated with the MATLAB software package.

### 3 Results

---

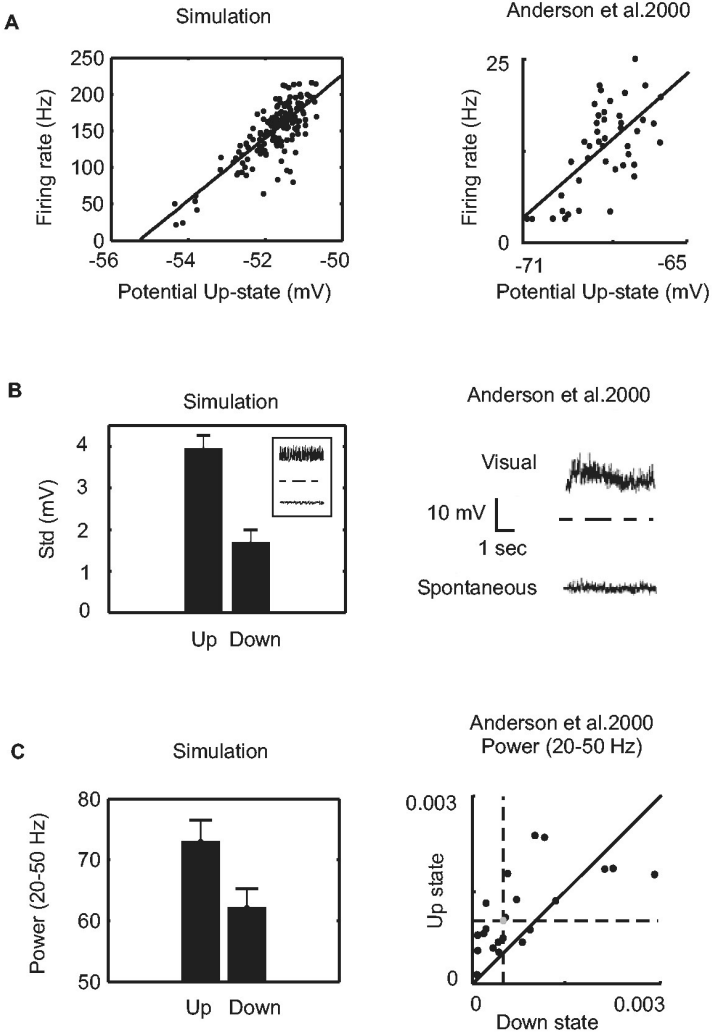
**3.1 Emergence of Up and Down States.** When we provide the model neuron with correlated inputs as explained, the membrane potential at the soma is characterized by up and down states of the dynamics (see Figures 2A and 2B, left panels). However, when the cell is stimulated with uncorrelated background activity, this bistability of the dynamics disappears (see Figure 2C, left panel). Indeed, in physiological recordings in primary visual cortex using stimulation paradigms that are not associated with correlation structures (awake cats during spontaneous activity), up and down states are not observed (Anderson et al., 2000; Steriade et al., 2001; see Figure 2C). When comparing the results of the simulation to recently published data (Azouz & Gray, 2003) the similarities are obvious. Compared to other experimental studies, however, a remarkable difference in timescales is apparent (see Figure 2A). In the purely passive model, the duration of the up states is typically around 30 ms, which is at least a factor of 10 lower than the experimental value. As discussed in Wilson and Kawaguchi (1996), the duration of the up and down states is mainly determined by the kinetic properties of  $\text{Ca}^{2+}$  and  $\text{Ca}^{2+}$ -dependent  $\text{K}^{+}$  currents. Including these active mechanisms in our model shows that this also holds true in the simulation (see Figure 2D). In comparison to the passive model, the duration of up states

increases by a factor of 10. It reaches a duration of 300 ms, resulting in an improved match to the experimental results.

**3.2 Quantification of Intracellular Dynamics.** To analyze the relationship between network and single cell dynamics in a more quantitative way, we compare a number of characteristic measures of the simulated neuron to known physiological results (Anderson et al., 2000). First, as reported in the literature, we find a significant correlation between the membrane potential in the up state and the spiking frequency (see Figures 2E and 3A). In Figure 2E, the calcium dynamics exerts its modulating effect by compressing the dynamic range for the firing frequency of the up states. The range is reduced from 10 to 220 Hz as in the passive case (see Figure 3A), to 5 to 50 Hz when calcium is introduced (see Figure 2E). Second, we find an increase of the standard deviation of the membrane potential in the up-state that matches that observed in the visual cortex (see Figure 3B). This is a large (more than twofold) and highly significant effect. The significance holds also in the comparison between the variability of the membrane potential during a simulated visual stimulation

---

Figure 3: *Facing page.* Characteristic features of up states and down states. (A) The firing rate in the up state (vertical axis) is shown as a function of the membrane potential in the up state (horizontal axis) for both the simulation of a passive model (left) and the experimental data (right). In both cases, the average membrane potential in the up state is correlated with the firing rate of the cell in the up state. The difference in the scale between the left and right panels depends on the mean input-firing rate chosen for this specific data set. The input correlation strength is 0.1, and the mean firing rate of the input is 85 Hz. See Figures 2D and 2E for a comparison of the active model with the experimental data. (B) The standard deviation (STD) of the membrane potential of the simulated neuron is increased in the up state as compared to the down state (left). The inset shows the subthreshold dynamics during stimulation and spontaneous background activity, respectively. The corresponding experimental data are shown to the right. In both cases, stimulation increases the variance of the subthreshold membrane potential. (C) The plot of the power spectra in the 20–50 Hz frequency band of the membrane potential for the optimal stimulation condition (left panel) shows an increase in the up state as compared to the down state. The same phenomenon is visible in the plot of the experimental data (right panel). Because no information is available on the normalization used for the power spectra in Anderson et al. (2000), we use arbitrary units, and a comparison of the absolute scale in the two panels is not possible. The vertical and horizontal dotted lines indicate the median for each corresponding axis; the light gray circle is the center of gravity of the distribution for a better comparison with the result of the simulation as shown in the left panel. The input pairwise correlation strength is 0.1 in Figures 3A and 3C and 0.2 in Figure 3B, while the mean input rate is always 85 Hz.



and spontaneous activity (see the Figure 3B inset and right panel). Finally, we observe an increase of the power in the 20 to 50 Hz frequency band in the up state versus the down state (see Figure 3C). This is a smaller effect, but it is still statistically significant and is comparable to reported experimental findings (see Figure 3C, right panel). These three results match experimental findings that some consider to be some of the central characteristics of up and down state dynamics (see Figures 3A to 3C, right side). Our results show that these characteristics emerge naturally in a detailed model of a cortical neuron when exposed to realistically structured input.

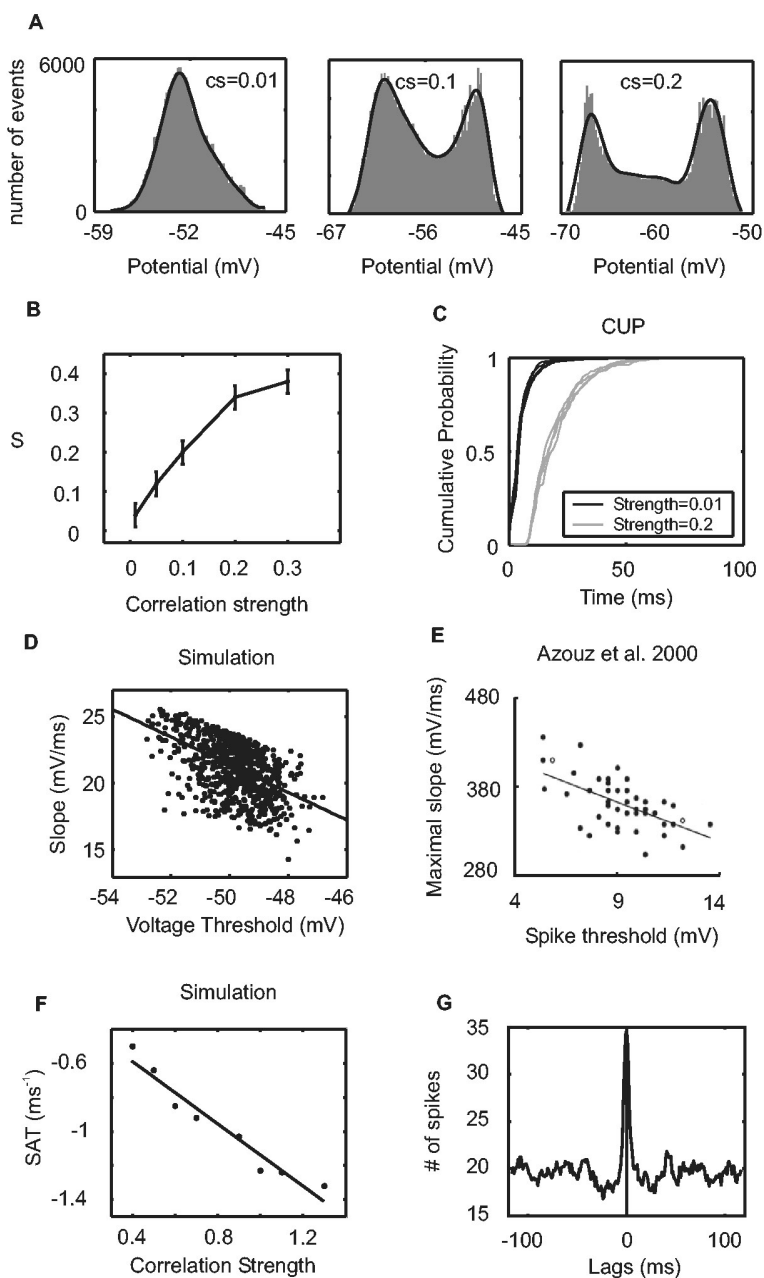
As a next step, we investigate measures of intracellular dynamics and relate them to the properties of the network's activity. We define a set of indices to capture different aspects of the subthreshold activity.

The first of these quantifies the strength of the correlations in the network activity and the bimodality of the membrane potential histogram. This a-dimensional index,  $S$ , accounts for the dependence of the bimodality on the input correlation strength:  $S = \frac{V_{\max} - V_{\min}}{|V_{\max}|}$ , where  $V_{\max}$  and  $V_{\min}$  are the location of the peaks in the membrane potential histograms (see Figures 2A and 2B). Increasing the correlation strength from its typically reported value of about 0.1 as used above (König et al., 1995a; Salinas & Sejnowski, 2000; Kock, Bernander, & Douglas, 1995) leads to an enhancement of the bimodality of the membrane potential histogram, resulting in a sharpening of the two peaks (see Figure 4A). This index is a monotonically increasing function of the correlation strength (see Figure 4B).

The next index represents the fraction of the total time spent in the up state (TUS). For each simulation, the total time the membrane potential surpassing the up threshold is divided by the total simulation time. This index is related to the integral of the peaks in the histograms, as explained in Anderson et al. (2000). The results indicate that this measure is strongly dependent on the input correlation strength. The TUS index is measured to be 7%, 13%, and 42% for the correlation strengths of 0.01, 0.1, and 0.2, respectively.

---

Figure 4: *Facing page*. Sensitivity of the membrane potential to the input correlation strength. (A) Histograms of the distribution of the membrane potential for three different conditions. The input correlation strength is increased from left to right: 0.01, 0.1, and 0.2, respectively. Bimodality emerges, and the hyperpolarized peak gets further away with increasing correlation strength. (B) The "S" index (see section 2), which quantifies the increasing separation of the peaks in the membrane potential histograms, is shown for five choices of correlation strengths. Note that the data points are connected by lines simply to improve visualization. We have no a priori hypotheses about specific functional relationships. (C) Cumulative probability distribution of the time intervals during which the membrane potential dwells above the up threshold. It is shown for six trials at two levels of correlation strength each. (D) For each action potential of the simulated neuron, the maximum slope of the rising phase of the membrane potential and the threshold potential for the spike generation are shown in a scatter plot. (E) The identical measure used in an experimental study demonstrates an inverse relationship as well. (F) The slope of the corresponding linear fit (solid line in Figure 4D), provides an index that is related to the input correlation strength. (G) To perform a reverse correlation analysis for every transition from down states to up states, a time window was centered in the corresponding population (PSTH) at the input stage to identify presynaptic events associated to the transition. The plot shows the average population activity in the temporal vicinity of a down-to-up transition.



The third measure relates the correlation strength of the inputs and the cumulative probability (CUP) distribution of the up state (Anderson et al., 2000). The cumulative probability distributions of the time intervals during which the membrane potential is above the up threshold are computed for different values of the input correlation strengths. Though it is not independent from the TUS index, it is a refinement of the previous index in that it controls for possible artifacts due to the spike-cutting procedure (see Figure 4C). The CUP measure can easily separate the diverse input correlation strengths, that is, 0.01 pairwise correlation strength (black lines) from 0.2 pairwise correlation strength (light gray lines).

Finally, the fourth index measures the slope at threshold (SAT) and thus characterizes the relationship between the input correlation structure and the dependence of the voltage threshold for the spike generation on the maximum slope of the rising phase of an action potential (see Figures 4D and 4E). Indeed, Azouz and Gray (2000) have observed an inverse relationship between the maximum slope of the rising phase of an action potential and the voltage threshold for the generation of the spike (see Figure 4E). A similar inverse relationship also appears in the simulated neuron (see Figure 4D). More important, we find that the slope of the fit quantifying the relationship between the maximum slope of the rising phase of an action potential and the voltage threshold for the generation of the spike provides a measure of the input correlation strength (see Figure 4F). This result indicates that this index tends to decrease with increasing correlation strength.

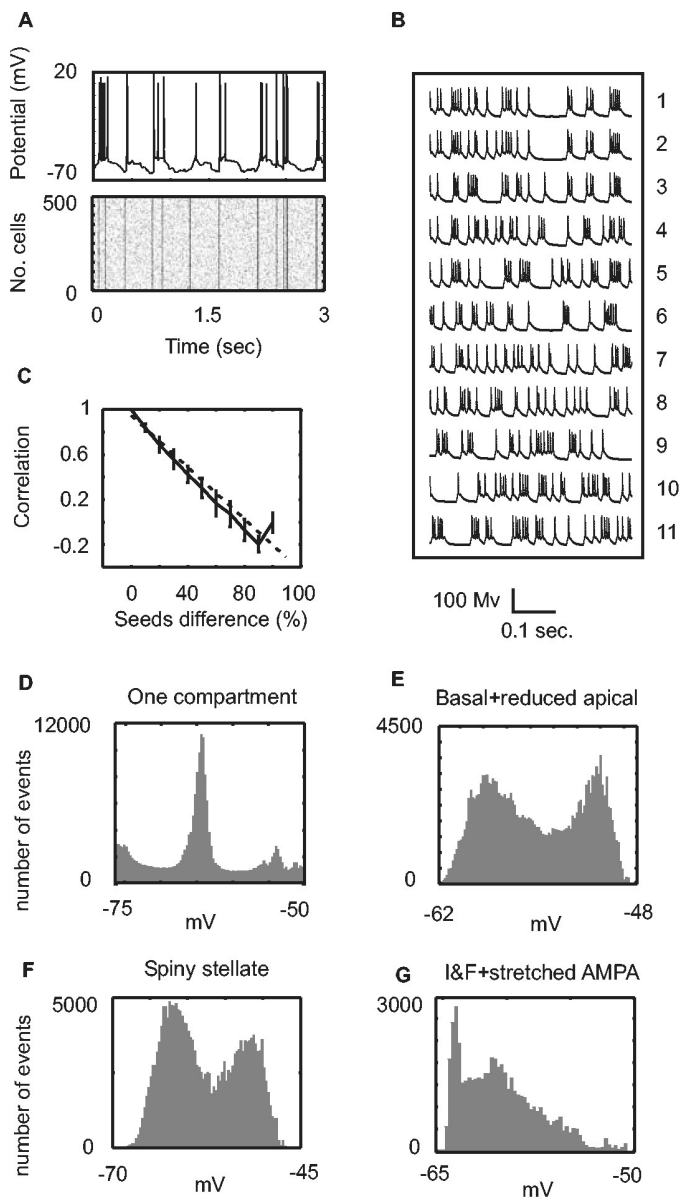
These analyses in the simulation data suggest that these four indices based on the membrane potential measurable within a single neuron can be used to extract the correlation strength within the network activity from the intracellular dynamics.

We focus now on the mechanisms of the observed bimodality. An important result comes from performing reverse correlation analysis of the transition from down to up states with respect to the population activity. On average, the total presynaptic activity around the transition from down to up states shows a sharp peak (see Figures 4G and 5A). This indicates that the switch of the intracellular dynamics between up and down states is induced by short, lasting, highly correlated input events. This confirms that up states are induced by presynaptic higher-order events. When the pairwise correlation strength is lowered, the amplitude of these sharp correlation peaks decreases, and the bimodality smoothly disappears. This is true for the passive L5 pyramidal cell, as well as for the model with voltage-dependent mechanisms. As shown before, the quantitative features differ in the two cases (duration of up states, or mean firing rate, for example), but the bimodality itself is not affected. Moreover, there is no intrinsic bimodality in the modeled neuron; the dynamics is fully input driven. When high-order correlation events disappear following a decrease in the pairwise correlations, the bimodality is destroyed, even though the mean input firing rate to the neuron is kept constant.

**3.3 Simulating Network Effects.** According to the above findings, up and down state fluctuations could manifest themselves in a large-scale coherent fashion if all the neurons in the population experience the same correlated dynamics (as for up and down fluctuations observed in slow-wave sleep states or in anesthetized conditions; see section 4). Instead, groups of neurons exposed to different network correlation structures would undergo different subthreshold dynamics. We tested this idea by running 11 different simulations of a neuron exposed to a corresponding number of different sets of input spike trains. While the mean firing rate and pairwise correlation strength were kept constant, the timing of the epochs used to generate the correlations was linearly changing: from identical for the first set to completely different for the last set. In other words, the timing of high-order correlation events, as highlighted by the reverse correlation analyses, was getting more and more dissimilar from set to set. For the first six sets, we observe a significant correlation between the membrane potentials of the simulated neurons ( $p < 0.001$ ). When the afferent signals are only slightly overlapping, the membrane potentials are no longer significantly correlated. High values of correlation, as experimentally described, are observed only when pairs of cells share a large fraction of synaptic inputs (see Figure 5B).

**3.4 Cell morphology.** An important question is whether the detailed morphology of a neuron contributes to the emergence of up and down states and, if so, what the key properties involved are. We manipulate the gross morphological structure of the pyramidal cell in a series of experiments. First, we delete all morphological specificity of the pyramidal neuron by morphing the cell into a spherical, single compartment of equal surface, while keeping the firing-rate transfer function unchanged. This reduces the cell to a conductance-based integrate-and-fire (IF) model. This procedure has been done with and without  $\text{Ca}^{2+}$  and  $\text{Ca}^{2+}$ -dependent  $\text{K}^{+}$  currents. Second, we morph the cell into a three-compartment model (basal dendritic tree plus soma, proximal-apical dendritic tree, and distal-apical dendritic tree) that preserves dendritic voltage attenuation (Destexhe, 2001). Third, we morph only the basal part into an equivalent compartment while preserving the apical dendritic tree in detail. In all these cases, when exposed to the same inputs used in the simulation experiments described above, the up and down dynamics disappear (see Figure 5D).

Interestingly, when exposing the IF model to the same input statistics and using a parameter choice for the  $\text{Ca}^{2+}$  currents that was eliciting long-lasting bistability in the L5 pyramidal cell, we do not find any up and down states. Note that this does not imply that it is not possible to find a choice of parameters and input statistics such that bimodality would emerge. However, when we keep the morphology of the basal dendritic tree unchanged and reduce the apical part to a single equivalent compartment, the qualitative aspects of the bimodal intracellular dynamics are preserved (see Figure 5E). Thus, we find that in the passive model, an intact basal dendritic tree is the



---

Figure 5: *Facing page*. (A) Somatic intracellular recordings of the membrane potential showing up-down fluctuations. The modeled cell incorporates calcium dynamics. The raster plot of the corresponding input activity is shown in the bottom panel. High-order correlation events (darker vertical stripes) of a few tens of milliseconds duration induce transitions to the up states. The distribution in time of these correlated events is according to a Poisson process. Up-states' duration can be prolonged by increasing the frequency of high-order events, as it happens in the time window of 2 to 2.5 seconds. The same effect is obtained by increasing the calcium peak conductance and time constants (see controls in section 2), with the result of eventually merging all the up states shown in the figure into a single long-lasting up state. (B) Decorrelating the subthreshold dynamics: a template set of points in time (in the raster plot shown in panel A, such a set of points would correspond to the moments in time when the vertical stripes occur) has been used to generate 10 other different sets of points, whose numeric values differ more and more from the original one. The first set is a perfect copy of the original template; the second one has 10% difference, and so on. The last one is 100% different. This group of 11 sets is then used to generate 11 corresponding different ensembles of 5000 correlated inputs. These 11 populations have increasingly different degree of correlations between them, since they share fewer and fewer time epochs for generating pairwise correlations (see section 2). We run the simulations and recorded the voltage traces for 10 seconds of simulation time. The subthreshold dynamics of the second trace is identical to the first one (the template), while the following traces differ more and more. (C) To quantify the degree of decorrelation, we windowed each voltage trace using a 1 second time window, and for each segment, we computed the linear correlation coefficients between the reference trace and the following ones. By using the windowing procedure, we could get 10 different estimates of the correlation coefficients for every couple of voltage traces, thus deriving an estimate of the mean correlation values and standard deviations. "Seeds" in the abscissa refers to the points in time used to create the correlations (see section 2). (D) The histogram of the membrane potential for a single spherical compartment, preserving the original input-output firing-rate transfer function, shows a central predominant peak and two small satellite peaks. The more depolarized one is an effect of the spike-cutting procedure, and the more hyperpolarized one is a result of the after-spike hyperpolarization. (E) Histogram of the membrane potential with intact basal morphology and a reduced apical one, substituted by a single cylinder of equivalent surface. (F) Histogram of the membrane potential of a spiny stellate cell with active mechanisms included (see the text for details). (G) Bimodality in the histogram of the membrane potential of an IF neuron with modified EPSPs' rising and decaying time constants, 1 ms and 12 ms, respectively.

minimal condition necessary for the emergence of up and down states. The interesting observation here is that the parameter set that robustly produces bistability in an L5 pyramidal cell does not produce the experimentally observed bistability for a point neuron.

As a further test of the hypothesis that the cable properties of the basal dendritic tree are essential for the generation of up and down states, we test a model of a spiny stellate cell developed by Banit and Segev (personal communication, 2003). From the point of view of the gross morphological structure, this spiny stellate cell can be considered as a pyramidal cell without an apical dendritic tree. It thus resembles the morphological characteristics of the cell used in the latter control. It is as if, instead of an equivalent cylindrical compartment, the apical part had been “cut off.” Furthermore, this model contains a number of active mechanisms (see section 2). Because Banit and Segev used this model for a different purpose, we extended it with AMPA and GABA synapses supplying correlated afferent input as described above. In this simulation, using an alternative detailed model neuron with several voltage-dependent mechanisms (see section 2), the same bimodality appears (see Figure 5F). This demonstrates that the basal dendritic tree is an important morphological compartment for the induction of up and down states.

In order to investigate the role of the basal dendritic tree, we separate the effects of the interaction of many excitatory postsynaptic potentials (EPSPs) in the dendrites and the effects of electrotonic propagation on individual EPSPs by developing a neuron model, which retains some aspects of dendritic processing, but radically simplifies others. We increased the duration of the EPSPs in an IF model without any detailed morphology (i.e., a point neuron). We kept the total charge flow and the input correlation structure unchanged—a correlation strength of 0.1 and a modification of the rise and decay time constants and peak amplitude of the conductance change,  $g(t)$ —to keep the integral constant. Also in this simulation, up and down states emerge (see Figure 5G). It should be emphasized that the quantitative mismatch in the bimodality between Figure 5G and Figure 2B is not surprising since the models used are completely different: an L5 pyramidal cell with detailed morphology and a single geometrical point, IF neuron. The intuitive explanation is that in the real neuron, as well as in the detailed simulations, when a barrage of EPSPs occurs synchronously in several basal dendrites, these long, thin cables quickly become isopotential compartments, each simultaneously depolarizing the soma. Moreover, the temporal filtering properties of these cables have the net effect of prolonging the effective duration of the EPSPs. Note that this temporal broadening is effective even though the intrinsic dendritic time constant,  $\tau$ , is lowered by the arrival of massive excitations, which increases the conductance (Paré, Shink, Gandreaux, Destexhe, & Lang, 1998). The overall effect is a strong, sustained current to the soma. We conclude that for the passive model, higher-order events, which naturally result from weak pairwise correlations in the network, combined

with physiologically realistic electrotonic dendritic properties, explain the bimodal distribution of the membrane potential and that active conductances shape its detailed temporal properties.

#### 4 Discussion

---

Here we show in a detailed model of a pyramidal neuron that weak pairwise correlations in its inputs, in combination with the electrotonic properties of its basal dendritic tree, cause up and down states in its membrane potential dynamics. Furthermore, several experimental characterizations of up and down states, such as an increase in gamma power and standard deviation of the membrane potential, can be explained in terms of presynaptic correlation structures. By introducing several statistical indices, we demonstrate a way to derive the correlation strength of the inputs, and thus in the activity of the network, from the subthreshold dynamics of a single neuron. In this sense, correlated activity in the network and the bimodality of the membrane potential are different views on one and the same phenomenon.

Previous explanations of up and down states have focused on a presynaptic origin and have suggested that synchronous barrages of excitations may be the major agents involved (Wilson & Kawaguchi, 1996). What kind of mechanism in the cortex could be responsible for their generation is an issue that has not been fully resolved. Here we show that no additional hypothesis other than the well-described weak pairwise correlations is required to fill this gap. However, we also show in our model that such a presynaptic source can account for the bimodality in the membrane potential of the postsynaptic neuron only when it is complemented by temporal filtering of the input spike trains by the basal dendrites. Active intracellular mechanisms sustain the triggered transitions to up states. Importantly, the neuron exhibits bimodality in its membrane potential with, as well as without, insertion of voltage-dependent mechanisms. The key effect of  $K^+$ -dependent  $Ca^{2+}$  or  $Na^+$  channels is their strong modulation of the quantitative properties of the subthreshold dynamics. This includes a sixfold compression of the dynamics range of the up state's mean firing rates. Potassium-dependent calcium and sodium channels can stretch the up-state duration from 25 to 300 ms, providing a better match with electrophysiological data. However, they are not responsible for the emergence of the phenomenon *per se*.

The differential impact of the morphology of the basal and apical dendrites on the response properties of pyramidal cells has been pointed out in other experimental (Larkum, Zhu, & Sakmann, 1999; Berger, Larkum, & Luscher, 2001) and theoretical studies (Körding & König, 2001). In these studies, properties of the inputs play a key role in the interaction of apical and basal dendritic compartments. In another study, it has been shown that the dynamic regulation of the dendritic electrotonic length can give rise to highly specific interactions in a cortical network that can account for the differential processing of multiple stimuli (Verschure & König, 1999).

**4.1 The Scope of the Model.** In our simulations, we do not reconstruct a complete visual system but approximate the first- and second-order statistical structure of the afferent inputs to a single neuron derived from experimental results. This approximation can be experimentally verified by intracellular recordings in area 17 of an anesthetized cat using full field gratings as visual stimuli. This setup has been used in a fair number of laboratories to demonstrate the existence of weak pairwise correlations in neuronal activity (Bair, 1999). Such synchronized activity has been observed over a spatial extent of several millimeters, roughly matching the scale of monosynaptic tangential connections in the cortex (Singer, 1993). Therefore, a pyramidal neuron in visual cortex samples mainly the activity of a region where neuronal activity is weakly correlated. Furthermore, the pyramidal cell reconstructed and simulated in this study has been recorded from and filled in primary visual cortex. Pyramidal cells are the predominant neuronal type in the whole cortex, and weak pairwise correlations have been found in many other cortical areas and species as well (Bair, 1999). Thus, our simulations apply to widely used experimental paradigms.

Another important question pertaining to our study and the physiological data it relates to is whether the phenomena studied here generalize to the awake, behaving animal. The impact of the behavioral state on the cortical dynamics is not fully understood, and the bulk of physiological experiments are performed under anesthesia. Electroencephalogram data show marked differences in the neuronal dynamics between different behavioral states (Steriade et al., 2001), and we can expect that the detailed dynamics of neuronal activity are affected. Furthermore, it is known that anesthetics influence the dynamics of up and down states during spontaneous activity (Steriade, 2001). However, whether the subthreshold dynamics is influenced by anesthetics when visual stimuli are applied is yet unknown. Furthermore, in the few studies where awake cats are used (Gray & Viana di Prisco, 1997; Siegel, Kording, & König, 2000), correlated activity on a millisecond timescale has been observed, compatible with the results obtained with the anesthetized preparation. Interestingly, a bimodality in the subthreshold dynamics has been observed in slow-wave sleep (Steriade et al., 2001). This raises the question of how the correlation structure of neuronal activity during sleep matches that observed under anesthetics. Hence, whether the assumptions made in our study, and the data they are based on, generalize to awake or sleeping animals has to be further investigated. The few results available suggest, however, that the relationship reported here between network dynamics and up down states could be valid for different behavioral states.

**4.2 Simplifications and Assumptions.** The simulations presented in this study incorporate a number of assumptions and simplifications. Although within the framework of the simulation, it is possible to use statistical indices to quantify the relationship between membrane potential dy-

namics and the statistical structure of the inputs, a full quantitative match between experimental and simulation results is difficult to achieve. To understand the reasons behind these differences (for standard deviation, see Figure 3B; for slope, see Figures 4D and 4E), it has to be considered that we investigated detailed compartmental models where many known channels and currents (Wilson & Kawaguchi, 1996) have been omitted. In particular, voltage-dependent currents with long time constants are known to play an important role in stabilizing and prolonging up and down states (Wilson & Kawaguchi, 1996). Once the upward or downward transition has occurred, active currents contribute to stabilizing the membrane potential in either an up state or a down state. Their duration is related not only to the input dynamics but also to the kinetic properties of such active mechanisms, which essentially implement a bistable attractor of the dynamics. Without that, the passive filtering properties of the dendrites would simply be responsible for the emergence of stretched-in-time envelopes of the coherent presynaptic events. Up and down states would be triggered but not maintained for prolonged periods. These considerations have been validated by a tenfold increase in the duration of the up states as soon as  $\text{Ca}^{2+}$  and  $\text{K}^{+}$ -dependent  $\text{Ca}^{2+}$  currents have been included in the model. The relative importance of voltage-dependent mechanisms and presynaptic events in inducing and maintaining a bistable neuronal dynamics seems to vary considerably depending on the animal and brain area. In view of this, the temptation to include a much larger number of active mechanisms to capture this complexity arises. However, it is quickly obvious that the data needed to specify the precise distribution and strength of each mechanism are not available. Therefore, the number of free parameters of the model, to be fitted by reaching a consistent input-output firing rate and other constraints, is dramatically increased and surpasses the number of constraints available.

An interesting alternative to the above scenario can be envisioned. Instead of increasing the complexity of the modeled cell, it is possible to lower the complexity of the real cell. Essentially, an experiment can be designed in which the focus shifts from an investigation of the cellular properties of the recorded neuron as such, to using the neuron as a probe to investigate the correlation structure in the network. The main guidelines of the experiment should be to record intracellularly from a neuron in primary visual cortex while presenting different visual stimuli that will induce different correlation structures. Gratings are known to induce pairwise correlations while randomly moving dots lead to weak or no correlations (Usrey & Reid, 1999; Brecht, Goebel, Singer, & Engel, 2001; Gray et al., 1990). Alternatively, synchronous network activity could be simulated by using an intracortical electrode and applying short, lasting, depolarizing current pulses. Applying blockers of voltage-dependent channels or hyperpolarizing the neuron strongly affects the membrane conductance and simplifies the dynamics within the real neuron. The aim is to reduce as much as possible the impact

of active mechanisms so that the real cell becomes simply a passive receiver of the input spike trains and their higher-order correlation statistics. Reducing the number of parameters that can vary in a real experiment to the smaller set of controlled parameters employed in the simulation study allows further validation of the conclusions derived from our model against physiological reality. This makes it possible to infer the correlation strength of the activity in the cortical network from the subthreshold dynamics as quantified by the indices described above. In this sense, the simulation study facilitates a new experimental approach, using a neuron under nonphysiological conditions as a passive probe to investigate the dynamics of the network.

## Appendix

---

The tables describe parameter values used in the NEURON simulation. "Place" (in Table 1) refers to the dendritic location of the inserted mechanism: "dendrites" indicates both basal and apical dendrites, while  $\bar{G}$  (and  $\bar{g}$  for synaptic mechanisms) indicate the peak conductance values. For Ih channels, the peak conductance varies according to the dendritic location, as reported by Berger et al. (2001). The parameters  $m$  and  $n$  refer to the kinetic scheme of the Hodgkin- and Huxley-like formalism used to describe the activation and inactivation properties of voltage dependent mechanisms, according to the following equation:

$$I_A = \bar{G}_A \times m_A^p \times n_A^q (u - E_A),$$

where  $A$  is a generic ionic type. The parameters  $k$  and  $u_{1/2}$  refer to the Boltzman equation that describes the steady-state conductance behavior of the ionic mechanisms inserted, according to the equation

$$f(u) = \frac{1}{1 + \exp\left(\frac{u_{1/2} - u}{k}\right)}.$$

Finally, the time course of the synaptic conductance (AMPA and GABA; see Table 2) follows an alpha function behavior:

$$f(t) = \exp\left(-\frac{t}{\tau_1}\right) - \exp\left(-\frac{t}{\tau_2}\right).$$

NMDA channels have been used solely in control experiments (see section 2.6).

## Acknowledgments

---

This work was supported the Swiss National Fund (31-61415.01), ETH Zürich and EU/BBW (IST-2000-28127/01.0208-1).

## References

---

- Agmon-Snir, H., & Segev, I. (1993). Signal delay and input synchronization in passive dendritic structures. *J. Neurophysiol.*, *70*, 2066–2085.
- Anderson, J., Lampl, I., Reichova, I., Carandini, M., & Ferster, D. (2000). Stimulus dependence of two-state fluctuations of membrane potential in cat visual cortex. *Nature Neurosci.*, *3*, 617–621.
- Azouz, R., & Gray, C. M. (2000). Dynamic spike threshold reveals a mechanism for synaptic coincidence detection in cortical neurons in vivo. *PNAS*, *97*, 8110–8115.
- Azouz, R., & Gray, C. M. (2003). Adaptive coincidence detection and dynamic gain control in visual cortical neurons in vivo. *Neuron*, *37*, 513–523.
- Bair, W. (1999). Spike timing in the mammalian visual system. *Curr. Opin. Neurobiol.*, *9*, 447–453.
- Benucci, A. Vershure, P. F., & König, P. (2003). Existence of high-order correlations in cortical activity. *Phys. Rev. E*, *68* (4 Pt 1), 041905.
- Berger, T., Larkum, M. E., & Luscher, H. R. (2001). High I(h) channel density in the distal apical dendrite of layer V pyramidal cells increases bidirectional attenuation of EPSPs. *J. Neurophysiol.*, *85*(2), 855–868.
- Bernander, Ö., Koch, C., & Douglas, R. J. (1994). Amplification and linearization of distal synaptic inputs to cortical pyramidal cells. *J. Neurophysiol.*, *72*, 2743–2753.
- Bernander, Ö., Koch, C., & Usher, M. (1994). The effects of synchronized inputs at the single neuron level. *Neural Computation*, *6*, 622–641.
- Bothé, S. M., Spekreijse, H., & Roelfsema, P. R. (2000). The effect of pair-wise and higher order correlations on the firing rate of a post-synaptic neuron. *Neural Computation*, *12*, 153–179.
- Brecht, M., Goebel, R., Singer, W., & Engel, A. K. (2001). Synchronization of visual responses in the superior colliculus of awake cats. *Neuroreport*, *12*, 43–47.
- Contreras, D., & Steriade, M. (1995). Cellular basis of EEG slow rhythms: A study of dynamic corticothalamic relationships. *J. Neurosci.*, *15*, 604–622.
- Dean, A. F. (1981). The variability of discharge of simple cells in the cat striate cortex. *Exp. Brain Res.*, *44*(4), 437–440.
- Destexhe, A. (2001). Simplified models of neocortical pyramidal cells preserving somatodendritic voltage attenuation. *Neurocomputing*, *38–40*, 167–173.
- Destexhe, A., & Paré, D. (1999). Impact of network activity on the integrative properties of neocortical pyramidal neurons in vivo. *J. Neurophysiol.*, *81*, 1531–1547.
- Destexhe, A., & Paré, D. (2000). A combined computational and intracellular study of correlated synaptic bombardment in neocortical pyramidal neurons in vivo. *Neurocomputing*, *32–33*, 113–119.
- Douglas, R. J., & Martin, K. A. C. (1990). Neocortex. In G. M. Shepherd (Ed.), *The synaptic organization of the brain* (pp. 389–438). Oxford: Oxford University Press.
- Douglas, R. J., Martin, K. A. C., & Whitteridge, D. (1991). An intracellular analysis of the visual responses of neurons in cat visual cortex. *J. Physiol. (London)*, *440*, 659–696.

- Engel, A. K., König, P., Gray, C. M., & Singer, W. (1990). Stimulus-dependent neuronal oscillations in cat visual cortex: Inter-columnar interaction as determined by cross-correlation analysis. *Eur. J. Neurosci.*, *2*, 588–606.
- Feng, J., & Brown, D. (2000). Impact of correlated inputs on the output of the integrate-and-fire model. *Neural Comput.*, *12*, 671–692.
- Gabbott, P. L., Martin, K. A. C., & Whitteridge, D. (1987). Connections between pyramidal neurons in layer 5 of cat visual cortex (area 17). *J. Comp. Neurol.*, *259*, 364–381.
- Gray, C. M., Engel, A. K., König, P., & Singer, W. (1990). Stimulus-dependent neuronal oscillations in cat visual cortex: Receptive field properties and feature dependence. *Eur. J. Neurosci.*, *2*, 607–619.
- Gray, C. M., & Viana di Prisco, G. (1997). Stimulus-dependent neuronal oscillations and local synchronization in striate cortex of the alert cat. *J. Neurosci.*, *17*, 3239–3253.
- Grün, S., Diesmann, M., & Aertsen, A. (2001). Unitary events in multiple single-neuron spiking activity: I: Detection and significance. *Neural Computation*, *14*, 43–80.
- Hines, M. L., & Carnevale, N. T. (2001). NEURON: A tool for neuroscientists. *Neuroscientist.*, *7*, 123–135.
- Kasanez, F., Riquelme, L. A., & Murer, M. G. (2002). Disruption of the two-state membrane potential of striatal neurones during cortical desynchronization in anesthetized rats. *J. Physiol.*, *543*, 577–589.
- Kisvarday, Z. F., Toth, E., Rausch, M., & Eysel, U. T. (1997). Orientation-specific relationship between populations of excitatory and inhibitory lateral connections in the visual cortex of the cat. *Cerebral Cortex*, *7*, 605–618.
- Kock, C., Bernander, Ö., & Douglas, R. J. (1995). Do neurons have a voltage or a current threshold for action potential initiation. *J. Comput. Neurosci.*, *2*, 63–82.
- König, P. (1994). A method for the quantification of synchrony and oscillatory properties of neuronal activity. *J. Neurosci. Meth.*, *54*, 31–37.
- König, P., Engel, A. K., & Singer, W. (1995a). How precise is neuronal synchronization? *Neural Computation*, *7*, 469–485.
- König, P., Engel, A. K., & Singer, W. (1995b). Relation between oscillatory activity and long-range synchronization in cat visual cortex. *PNAS*, *92*, 290–294.
- Körding, K. P., & König, P. (2001). Supervised and unsupervised learning with two sites of synaptic integration. *J. Comput. Neurosci.*, *11*, 207–215.
- Lampl, I., Reichova, I., & Ferster, D. (1999). Synchronous membrane potential fluctuations in neurons of the cat visual cortex. *Neuron*, *22*, 361–374.
- Larkum, M. E., Zhu, J. J., & Sakmann, B. (1999). A new cellular mechanism for coupling inputs arriving at different cortical layers. *Nature*, *398*, 338–341.
- Lewis, B. L., & O'Donnell, P. (2000). Ventral tegmental area afferents to the prefrontal cortex maintain membrane potential “up” states in pyramidal neurons via D1 dopamine receptors. *Cerebral Cortex*, *10*, 1168–1175.
- Mazurek, M. E., & Shadlen, M. N. (2002). Limits to the temporal fidelity of cortical spike rate signal. *Nature Neurosci.*, *5*, 463–471.
- Mel, B. W. (1993). Synaptic integration in an excitable dendritic tree. *J. Neurophysiol.*, *70*, 1086–1101.

- Paré, D., Shink, E., Gaudreau, H., Destexhe, A., & Lang, E. J. (1998). Impact of spontaneous synaptic activity on the resting properties of cat neocortical pyramidal neurons in vivo. *J. Neurophysiol.*, *79*, 1450–1460.
- Roskies, A., et al. (1999). Reviews on the binding problem. *Neuron*, *24*(1), 7–110.
- Salin, P. A., & Bullier, J. (1995). Corticocortical connections in the visual system: Structure and function. *Physiological Rev.*, *75*, 107–154.
- Salinas, E., & Sejnowski, T. J. (2000). Impact of correlated synaptic input on output firing rate and variability in simple neuronal models. *J. Neurosci.*, *20*, 6193–6209.
- Salinas, E., & Sejnowski, T. J. (2001). Correlated neuronal activity and the flow of neural information. *Nat. Rev. Neurosci.*, *2*, 539–550.
- Shadlen, M. N., & Newsome, W. T. (1998). The variable discharge of cortical neurons: Implications for connectivity, computation and information coding. *J. Neurosci.*, *18*, 3870–3896.
- Siegel, M., Kording, K. P., & König, P. (2000). Integrating top-down and bottom-up sensory processing by somato-dendritic interactions. *J. Neurosci.*, *8*, 161–173.
- Singer, W. (1993). Synchronization of cortical activity and its putative role in information processing and learning. *Annu. Rev. Physiol.*, *55*, 349–374.
- Singer, W., & Gray, C. M. (1995). Visual feature integration and the temporal correlation hypothesis. *Annu. Rev. Neurosci.*, *18*, 555–586.
- Softky, W. R., & Koch, C. (1993). The highly irregular firing of cortical cells is inconsistent with temporal integration of random EPSPs. *J. Neurosci.*, *13*, 334–350.
- Sompolinsky, H., & Shapley, R. (1997). New perspectives on the mechanisms for orientation selectivity. *Current Opinion in Neurobiol.*, *7*, 514–522.
- Steriade, M. (2001). Impact of network activities on neuronal properties in corticothalamic systems. *J. Neurophysiol.*, *86*, 1–39.
- Steriade, M., Contreras, D., & Amzica, F. (1994). Synchronized sleep oscillations and their paroxysmal developments. *Trends Neurosci.*, *17*, 199–208.
- Steriade, M., Timofeev, I., & Grenier, F. (2001). Natural waking and sleep states: A view from inside neocortical neurons. *J. Neurophysiol.*, *85*, 1968–1985.
- Stern, E. A., Jaeger, D., & Wilson, C. J. (1998). Membrane potential synchrony of simultaneously recorded striatal spiny neurons in vivo. *Nature*, *394*, 475–478.
- Stern, E. A., Kincaid, A. E., & Wilson, C. J. (1997). Spontaneous subthreshold membrane potential fluctuations and action potential variability of rat corticostriatal and striatal neurons in vivo. *J. Neurophysiol.*, *77*, 1697–1715.
- Stroeve, S., & Gielen, S. (2001). Correlation between uncoupled conductance-based integrate-and-fire neurons due to common and synchronous presynaptic firing. *Neural Comput.*, *13*, 2005–2029.
- Usrey, W. M., & Reid, R. C. (1999). Synchronous activity in the visual system. *Annu. Rev. Physiol.*, *61*, 435–456.
- Verschure, P.F., & Knig, P. (1999). On the role of biophysical properties of cortical neurons in binding and segmentation of visual scenes. *Neural Comput.*, *11*, 1113–1138.

- Wilson, C. J., & Groves, P. M. (1981). Spontaneous firing patterns of identified spiny neurons in the rat neostriatum. *Brain Res.*, *220*, 67–80.
- Wilson, C. J., & Kawaguchi, Y. (1996). The origins of two-state spontaneous membrane potential fluctuations of neostriatal spiny neurons. *J. Neurosci.*, *16*, 2397–2410.

---

Received September 4, 2003; accepted April 7, 2004.